Short communication

High-rate cathodes based on $Li_3V_2(PO_4)_3$ nanobelts prepared via surfactant-assisted fabrication

Anqiang Pan [a,b], Daiwon Choi [b], Ji-Guang Zhang [b,*], Shuquan Liang [a,**], Guozhong Cao [c], Zimin Nie [b], Bruce W. Arey [b], Jun Liu [b,***]

[a] Department of Materials Science and Engineering, Central South University, Hunan 410083, People's Republic of China
[b] Pacific Northwest National Laboratory, Richland, WA 99352, USA
[c] University of Washington, Seattle, WA 98195, USA

ABSTRACT

In this work, we have synthesized monoclinic $Li_3V_2(PO_4)_3$ nanobelts via a single-step, solid-state reaction process in a molten hydrocarbon. The as-prepared $Li_3V_2(PO_4)_3$ nanoparticles have a unique nanobelt shape and are ~50-nm thick. When cycled in a voltage range between 3.0 V and 4.3 V at a 1C rate, these unique $Li_3V_2(PO_4)_3$ nanobelts demonstrate a specific discharge capacity of 131 mAh g^{-1} (which is close to the theoretical capacity of 132 mAh g^{-1}) and stable cycling characteristics.

© 2010 Elsevier B.V. All rights reserved.

1. Introduction

Because of their high energy density and long cycle life, secondary lithium (Li)-ion batteries are the power sources of choice for modern portable electronic devices. Due to the rapid depletion of nonrenewable fuels and the environmental impacts resulting from the use of these traditional fuels, secondary Li-ion batteries also are being used as alternative power sources for high-power applications, such as electrical vehicles (EV), including hybrid electrical vehicles (HEV). Recently, Li transition metal phosphates have attracted widespread interest among researchers because of their appealing crystal structural features (e.g., good electrochemical and thermal stability and high operation potentials) [1–5]. Padhi et al. [1] worked on increasing the $Fe^{2+/3+}$ redox couple potential of $LiFePO_4$ through the inductive effect of polyanions in the phospho-olivine cathode. Subsequently, significant efforts have focused on overcoming the major obstacle of low ionic/electronic conductivity of $LiFePO_4$ by developing nano-sized cathode particles with inti-

mate conductive coatings. These efforts have led to $LiFePO_4$-based, Li-ion batteries for high-power applications, including power tools and EVs [6,7].

With the successful commercialization of $LiFePO_4$, other Li transition metal phosphates also have attracted attention. One example is $Li_3V_2(PO_4)_3$, which consists of a three-dimensional framework of slightly distorted VO_6 octahedral- and PO_4 tetrahedral-sharing oxygen vertexes that house Li ions in relatively large interstitial sites [2,8–10]. $Li_3V_2(PO_4)_3$ also has exceptional ionic conductivity that results from the large interstitial spaces created by the PO_4^{3-} units, which allow fast migration of ions in any direction. Compared with an olivine-type structure and the curved one-dimensional, channel-structured $LiFePO_4$, monoclinic $Li_3V_2(PO_4)_3$ exhibits a much higher Li-ion diffusion efficiency and higher intercalation potentials. Rui et al. [8] reported that the diffusion coefficient, D_{Li+} (from 10^{-9} to 10^{-10} cm^2 s^{-1}), of $Li_3V_2(PO_4)_3$ is five orders of magnitude higher than that of $LiFePO_4$ reported by Prosini et al. [11] (10^{-14}–10^{-16} cm^2 s^{-1}), which indicates that $Li_3V_2(PO_4)_3$ has great potential to achieve a higher rate capability than $LiFePO_4$. The highest capacity among the Li metal phosphates (197 mAh g^{-1}) can be reached [8] when three Li^+ ions are totally extracted from the lattice of $Li_3V_2(PO_4)_3$ when charging between 3.0 V and 4.8 V. However, the intrinsic low electronic conductivity of $Li_3V_2(PO_4)_3$ (2.4×10^{-7} S cm^{-1} at room temperature) largely limits its rate performance. Various synthesis and processing approaches, such

as alien metal doping and carbon coating [8,12–15] have been employed to mitigate this problem.

Nanotechnologies have been widely used in the preparation of electrode materials for Li-ion batteries to improve battery performance. Compared to micro-sized materials, nano-sized materials exhibit much shorter Li-ion diffusion and electron-transportation distances, both of which will greatly enhance the rate capability [16,17]. Although nano-sized electrodes have many advantages, multiple-step preparation processes often are needed to carefully control the particle sizes and prevent aggregation of large particles. Recently, Choi et al. [3] reported the one-step synthesis of LiMnPO$_4$ nanoplates via solid-state reaction in molten surfactant-paraffin media, which is a process that combines both the advantages of solid-state and self-assembling approaches. Oleic acid with one high polarity attached to the precursors and a polar tail extending to the molten solvent paraffin, plays a critical role in preventing agglomeration by steric hindrance during formation of LiMnPO$_4$ nanocrystals.

For cathode materials, low-temperature chemical routes are not suitable because the electrochemical response strongly depends on the crystallinity of the material. Therefore, a solid-state reaction is preferred over low-temperature routes. However, to improve the rate performance, a nanomaterial is required. Our molten surfactant-paraffin approach can satisfy these requirements in a single step and can be applied to not only LiMnPO$_4$ but other cathode materials such as Li$_3$V$_2$(PO$_4$)$_3$. In this paper, we describe a one-step preparation procedure for fabricating nanobelt structured Li$_3$V$_2$(PO$_4$)$_3$. The procedure is based on a solid-state reaction in a molten surfactant-paraffin media. The particles in the resulting Li$_3$V$_2$(PO$_4$)$_3$ nanobelts are uniform in size and are well dispersed. We discuss the electrochemical performance of this material under different charge/discharge conditions in the paper. The microstructures of the material also were characterized using various microscopic techniques and were correlated with their high-rate charge/discharge performances.

2. Experimental

V$_2$O$_5$, NH$_4$H$_2$PO$_4$, LiCOOCH$_3$·2H$_2$O, oxalic acid, oleic acid, and paraffin wax were used as received without further purification. First, V$_2$O$_5$ (99.6%, Alfa Aesar) and oxalic acid (>99% RT, Sigma–Aldrich) in a stoichiometric ratio of 1:3 were added to deionized water that was magnetically stirred at room temperature until a clear blue solution formed. Water was evaporated from the solution to yield the VOC$_2$O$_4$·nH$_2$O for further use. For Li$_3$V$_2$(PO$_4$)$_3$ nano-belt synthesis, LiCOOCH$_3$·2H$_2$O (reagent grade, Sigma), self-prepared VOC$_2$O$_4$·nH$_2$O (as mentioned above), NH$_4$H$_2$PO$_4$ (99.999%, Sigma–Aldrich), oleic acid (FCC, FG, Aldrich), and paraffin wax (ASTMD 87, melting point 53 ∼57 °C, Aldrich) were used as precursors. NH$_4$H$_2$PO$_4$ was milled initially with oleic acid for 1.5 h in a high-energy mechanical mill (SPEX 8000 M) in a stainless steel vial. After the initial milling in oleic acid, the NH$_4$H$_2$PO$_4$ was milled further for 30 min with the paraffin wax. Then, the VOC$_2$O$_4$ was added, and the mixture was milled for 10 min. Finally, Li acetate was added and milled for another 10 min. The overall Li:V:P:oleic acid molar ratio of the milling mixture was 3:2:3:3 with the paraffin added in an amount twice the weight of the oleic acid. The resulting viscous liquid slurry mixture was dried in an oven at >100 °C for 30 min and subjected to heat treatment at 800 °C for 8 h under an ultra-high-purity argon atmosphere with a heating rate of 5 °C/min to make the final Li$_3$V$_2$(PO$_4$)$_3$ nanobelts. During the heat treatment process, the evaporated paraffin was collected at the cooler part of the tube furnace. The crystalline structure of the as-prepared sample was determined by X-ray diffraction (XRD) analysis using a Scintag XDS2000 θ–θ powder diffractome-
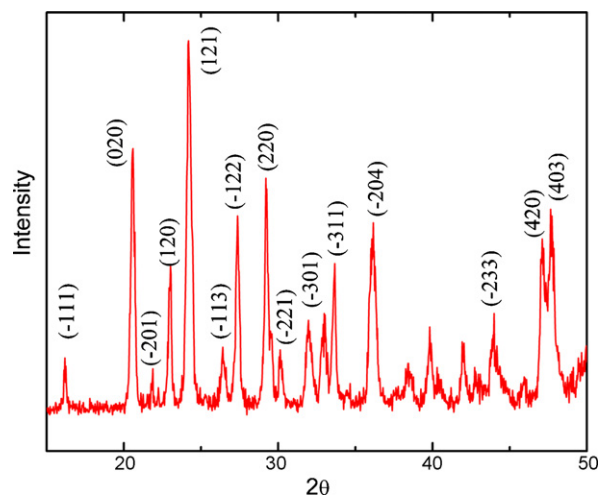

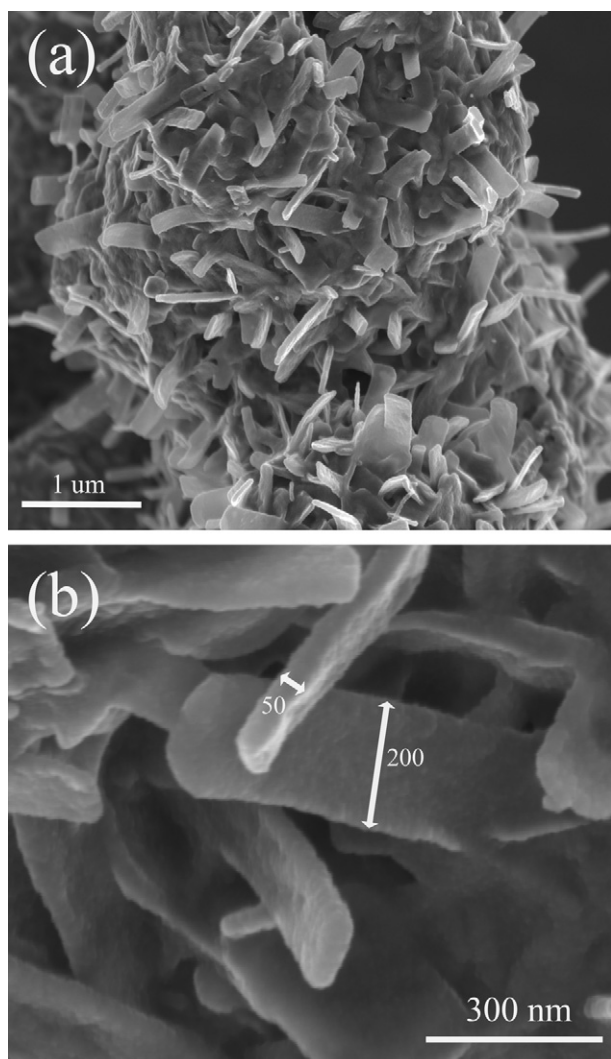**Fig. 1.** XRD pattern of the as-synthesized Li$_3$V$_2$(PO$_4$)$_3$/carbon sample.

ter equipped with a Ge (Li) solid-state detector and a Cu Kα sealed tube (λ = 1.54178 Å). The sample was scanned within the range of 10° and 70° (2θ), with a step size of 0.02° and an exposure time of 10 s. A focused-ion-beam scanning electron microscope (FIB-SEM) (FEI Helios 600 Nanolab FIB-SEM, 3 KV) was used to characterize the particle morphology.

The electrode slurry was prepared by mixing Li$_3$V$_2$(PO$_4$)$_3$, Super P conductive carbon (TIMCAL Graphite & Carbon) and poly(vinylidene fluoride) (PVDF) binder dispersed in an N-methylpyrrolidone solution at a weight ratio of 75:15:10, respectively. The slurry was spread on aluminum foil and dried in a vacuum oven at 100 °C overnight prior to coin-cell assembly. The half-cells (2325 coin cell, National Research Council, Canada) were assembled in a glove box (MBraun, Inc.) filled with ultra-high-purity argon. Polypropylene membrane (Celgard 3501) was used as a separator, Li metal was used as the anode, and 1-M LiPF$_6$ in ethyl carbonate/dimethyl carbonate (1:1, v/v ratio) was used as the electrolyte. The electrochemical performance of the Li$_3$V$_2$(PO$_4$)$_3$ was evaluated on an Arbin Battery Tester BT-2000 (Arbin Instruments, College Station, TX) at room temperature. The half-cells were tested within a voltage cutoff range of 3–4.3 V vs. Li/Li$^+$ at various charging rates based on the weight of the active material (assuming a 1C charging rate of 132 mA g^{-1}).
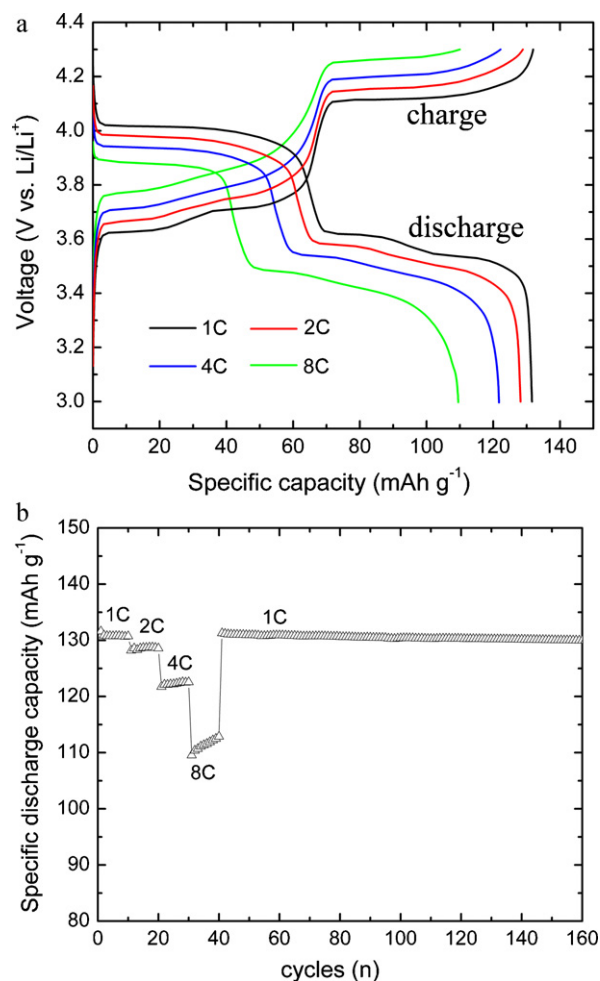
3. Results and discussion

The black color of the obtained material after calcination is attributed to the carbon produced from decomposition of oleic acid at high temperature. Fig. 1 shows the XRD pattern of the as-prepared Li$_3$V$_2$(PO$_4$)$_3$ sample. The main peaks are indexed, and all the peaks detected are aligned well with the space group P21/n (PDF: 01-072-7074) in monoclinic Li$_3$V$_2$(PO$_4$)$_3$, as well reported in the literature [8,18]. No carbon phase was detected, which indicates that the residual carbon in the composite is amorphous. According to our thermogravometric analysis results, the amount of residual carbon in the composite is about 2 wt.%.

Fig. 2 shows FIB-SEM images of uniformly dispersed Li$_3$V$_2$(PO$_4$)$_3$ nanobelts synthesized using the molten hydrocarbon procedure. The Li$_3$V$_2$(PO$_4$)$_3$ nanobelt is approximately 50-nm thick, 200-nm wide, and extends as long as 500 nm. As shown in Fig. 2(a), the nanobelt particles are homogenously dispersed, and the shape of the nanobelts is quite uniform. Although the aggregation is well defined because the nanobelts are sintered at high temperature (800 °C), the structure of the electrode material is still highly porous. Fig. 2(b) shows the nanobelt particles at higher

Fig. 2. FIB-SEM images of $Li_3V_2(PO_4)_3$ nanobelts at low (a) and high (b) magnifications.

Fig. 3. (a) Discharge/charge curves and (b) cycling performance at various C-rates with constant charge/discharge rate. Here 1C = 132 mAh g^{-1}.

magnification. To the best of our knowledge, this is the first time that nanobelt structures of $Li_3V_2(PO_4)_3$ have been synthesized. Because the nanobelts do not grow parallel to each other, a large space exists between each nanoparticle. The role of the oleic acid [(CH$_3$(CH$_2$)$_7$CH=CH(CH$_2$)$_7$COOH)], a mono-unsaturated omega-9 fatty acid found in animals and vegetables is to act as the surface-capping ligand of precursors with its carboxylic group, thereby preventing agglomeration by steric hindrance during formation of $Li_3V_2(PO_4)_3$ nanocrystals. Such an oleic acid surfactant can extend its tail in molten paraffin media in a manner similar to self-assembly. In this role, oleic acid acts as a surfactant that directs the growth orientation of $Li_3V_2(PO_4)_3$ nanobelts. Furthermore, the residual carbon from the decomposition of oleic acid on the active material also can facilitate electron transportation in the final $Li_3V_2(PO_4)_3$ product. The detailed formation mechanism of the nanostructures can be found in our recent publication on LiMnPO$_4$ nanoplate growth via solid-state reactions in molten hydrocarbon media [3]. Regarding differences in the morphologies of the two final products (i.e., nano-plates for LiMnPO$_4$, and nano-belts for $Li_3V_2(PO_4)_3$), the differences probably are caused by the inherent differences in the materials. Different materials with different crystal structures have different surface energies and thermodynamically preferred growth characteristics. Therefore, the shapes can vary.

Fig. 3 shows the discharge and charge curves and their cycling performance at various C rates when the samples were cycled between 3.0 V and 4.3 V vs. Li/Li$^+$. At 1C rate, three plateaus are observed on the charge curves at 3.62 V, 3.70 V, and 4.12 V, which can be attributed to the phase transition from x = 3.0 to 2.5, 2.0, and 1.0, respectively when Li$^+$ ions were extracted from $Li_xV_2(PO_4)_3$. The first Li$^+$ ion is extracted in two steps (at 3.62 V and 3.70 V) because of the existence of an ordered phase $Li_{2.5}V_2(PO_4)_3$ at a mixed V^{3+}/V^{4+} state [8]. Then, a single-step extraction of the second Li$^+$ ion at 4.12 V is observed; this extraction corresponds to the complete oxidation of V^{3+} to V^{4+}. Three corresponding plateaus at 4.0 V, 3.63 V, and 3.55 V during the discharge process are attributed to reinsertion of two Li ions, which accompanies the phase transition of $Li_xV_2(PO_4)_3$ from x = 1.0 to 2.0, 2.5, and 3.0, respectively. An initial discharge capacity of 131 mAh g^{-1} was detected, which is very close to the theoretical capacity of 132 mAh g^{-1} for $Li_xV_2(PO_4)_3$ (with the value of x ranging from 1 to 3) when cycled between 3 V and 4.3 V. After 10 cycles at a 1C rate (shown in Fig. 3(b)), the cell was reset at a 2C rate, and it delivered a specific discharge capacity of 128 mAh g^{-1}. When operated at 4C and 8C charge/discharge rates, the specific discharge capacities were still as high as 122 mAh g^{-1} and 110 mAh g^{-1}, respectively. Fig. 3(b) shows the cycling performance of a $Li_3V_2(PO_4)_3$ nanobelt electrode at various rates. After 40 cycles (shown in Fig. 3(b)), the electrode can restore a specific discharge capacity to 131 mAh g^{-1} when the rate is reset to 1C. This 131 mAh g^{-1} specific discharge capacity value is the same

as that observed after the first 10 cycles before charging at high rate. Between 40 and 160 cycles, only negligible capacity fading from 131 mAh g^{-1} to 130 mAh g^{-1} was observed. The excellent rate performance and good capacity retention at various discharge rates can be attributed to the nanobelt-structured, Li$_3$V$_2$(PO$_4$)$_3$. As rate performance is closely related to Li-ion diffusion in the electrode, the reduced size of the nanobelts (50-nm thick) certainly decreases the diffusion distance required for the Li ions. The large void space between each particle (shown in Fig. 2(b)) allows easy penetration of the electrolyte, which thus increases the interfacial surface area between the active material and the electrolyte. In addition, the residual carbon produced from the decomposition of oleic acid improves electron conductivity and thus facilitates electron transport. To the best of our knowledge, the electrochemical performance of this nanobelt-structured Li$_3$V$_2$(PO$_4$)$_3$ material is among the best ever reported. The preparation procedure developed in this work also is cost effective and is suitable for the large-scale production of batteries such as those used in EVs.

4. Conclusions

In this study, we synthesized Li$_3$V$_2$(PO$_4$)$_3$ nanobelts by solid-state reaction in a molten hydrocarbon. This preparation procedure is facile and uses inexpensive and safe oleic acid and paraffin additives. These additives create an environment that mimics the reverse-micelle approach in which uniform Li$_3$V$_2$(PO$_4$)$_3$ nanobelts are grown during a heat-treatment process. The morphologies of the nanobelts are uniform and well dispersed, thus creating porous secondary particles. Electrochemical tests of the nanobelts revealed good rate performance and excellent cycle stability. This good performance is attributed to the novel, open nanobelt structure of Li$_3$V$_2$(PO$_4$)$_3$; this open, nano-sized structure is advantageous because of (1) the reduced distance for Li-ion diffusion and electron transport among the belts and (2) the improved surface contact and the accelerated ion transfer between the electrode and the electrolyte. Finally, the facile method developed in this work also can be used in the development of other functional materials.

References

[1] A.K. Padhi, K.S. Nanjundaswamy, J.B. Goodenough, J. Electrochem. Soc. 144 (1997) 1188–1194.
[2] S.C. Yin, H. Grondey, P. Strobel, M. Anne, L.F. Nazar, J. Am. Chem. Soc. 125 (2003) 10402–10411.
[3] D. Choi, D. Wang, I.T. Bae, J. Xiao, Z.M. Nie, W. Wang, V.V. Viswanathan, Y.J. Lee, J.-G. Zhang, G.L. Graff, Z.G. Yang, J. Liu, Nano Lett. 10 (2010) 2799–2805.
[4] D. Choi, D. Wang, V.V. Vinawathan, I.-T. Bae, W. Wang, Z. Nie, Y.J.J. Lee, -G. Zhang, G.L. Graff, Z. Yang, J. Liu, T. Dong, Electrochem. Commun. 12 (2010) 378–381.
[5] A. Pan, J. Liu, J.-G. Zhang, W. Xu, G. Cao, Z. Nie, B.W. Arey, S. Liang, Electrochem. Commun. 12 (2010) 1674–1677.
[6] Y. Wang, Y. Wang, E. Hosono, K. Wang, H. Zhou, Angew. Chem. Int. Ed. (2008) 7461–7465.
[7] D. Choi, P.N. Kumta, J. Power Sources 163 (2007) 1064–1069.
[8] X.H. Rui, N. Ding, J. Liu, C. Li, C.H. Chen, Electrochim. Acta 55 (2010) 2384–2390.
[9] M.Y. Saidi, J. Barker, H. Huang, J.L. Swoyer, G. Adamson, Electrochem. Solid State Lett. 5 (2002) A149–A151.
[10] M.Y. Saidi, J. Barker, H. Huang, J.L. Swoyer, G. Adamson, J. Power Sources 119 (2003) 266–272.
[11] P.P. Prosini, M. Lisi, D. Zane, M. Pasquali, Solid State Ionics 148 (2002) 45–51.
[12] M.M. Ren, Z. Zhou, Y.Z. Li, X.P. Gao, J. Yan, J. Power Sources 162 (2006) 1357–1362.
[13] P. Fu, Y.M. Zhao, X.N. An, Y.Z. Dong, X.M. Hou, Electrochim. Acta 52 (2007) 5281–5285.
[14] J. Wang, J. Liu, G.L. Yang, X. Zhang, X. Yan, X. Pan, R. Wang, Electrochim. Acta 54 (2009) 6451–6454.
[15] S. Yang, Y. Song, P.Y. Zavalij, M.S. Whittingham, Electrochem. Commun. 4 (2002) 239–244.
[16] A. Pan, J.-G. Zhang, Z. Nie, G. Cao, B.W. Arey, G. Li, S. Liang, J. Liu, J. Mater. Chem. 20 (2010) 9193–9199.
[17] A. Pan, J. Liu, J.-G. Zhang, G. Cao, W. Xu, Z. Nie, X. Jie, D. Choi, B.W. Arey, C. Wang, S. Liang, J. Mater. Chem., doi:10.1039/c0jm02810j.
[18] P. Fu, Y.M. Zhao, Y.Z. Dong, X.N. An, G.P. Shen, J. Power Sources 162 (2006) 651–657.